Revisit Electrolyte Chemistry of Hard Carbon in Ether for Na Storage

Jun Pan
Shandong University
Yi-Yang Sun
Shanghai Institute of Ceramics
Yehao Yan
Jining Medical University
Lei Feng
Key laboratory of Colloid and Interface Chemistry
Yifan Zhang
Shanghai Institute of Ceramics
Aming Lin
Shanghai Institute of Ceramics
Fuqiang Huang (huangfq@mail.sic.ac.cn)
Shanghai Institute of Ceramics https://orcid.org/0000-0003-0526-5473
Jian Yang
Shandong University

Article

Keywords: batteries, energy storage, hard carbons (HC), Lithium-ion batteries (LIBs)

Posted Date: February 2nd, 2021

DOI: https://doi.org/10.21203/rs.3.rs-153133/v1

Abstract

Hard carbons (HC) as an anode material in sodium ion batteries, present enhanced electrochemical performances in ether-based electrolytes, making them promising potential in practical applications. However, the underlying mechanism behind the excellent performances is still in question. Here, ex-situ nuclear magnetic resonance, gas chromatography-mass spectrometry and high-resolution transmission electron microscope were used to clarify the insightful chemistry of ether- and ester-based electrolytes in terms of solid-electrolyte-interphase (SEI) on hard carbons. The results confirm the marked electrolyte decomposition and the formation of a SEI film in EC/DEC, but no SEI film in the case of diglyme. In-situ electrochemical quartz crystal microbalance and molecule dynamics support that ether molecules have been co-intercalated into hard carbons likely. To our knowledge, these results are reported for the first time. It might be very useful for us to rational design advanced electrode materials based HC in future.

Introduction

Lithium-ion batteries (LIBs) have achieved great successes in the past decades, but the limited resources of lithium greatly restrain the applications of LIBs in smart grids, electric vehicles, etc[1-3]. Therefore, replacing lithium by other elements is very necessary. Sodium ion batteries (NIBs) as one of the next-generation batteries well address this concern, due to the abundant reserves of sodium in earth. Moreover, NIBs share the similar basic fundamentals and fabrication protocols as LIBs[4-6]. However, the heavy mass and large size of Na ions greatly increase the redox overpotential and volume change of electrode materials, resulting in a reduced electrochemical activity and a marked structure instability. Thus, many electrode materials, which have been used in LIBs, do not work in NIBs. Graphite, a typical anode material in LIBs, only stores a small capacity of Na ions in carbonate electrolytes, due to the poor thermodynamic stability of Na-related intercalation compounds in graphite[7]. Using ether rather than carbonate as the electrolyte promotes a reversible capacity to ~150 mAh g^{-1}[8], where ether is co-intercalated together with Na ions into graphite. But this data is still worse than that in LIBs. Hard carbons (HC), whose structure is featured by numerous structure defects and micro-voids, and random-oriented graphene layers, present a large reversible capacity (300-400 mAh g^{-1}), and a low operation voltage (~0.1 V vs. Na^+/Na)[9]. Furthermore, this unique structure of HC also restrains the exfoliation of graphene layers caused by co-intercalation chemistry, benefiting the long-term cycling stability. Therefore, they are considered one of the promising anode materials of NIBs for practical applications.

However, the electrochemical performances of hard carbon are still far away to be satisfied so far. The main obstacles of hard carbons in NIBs come from the poor rate capability, the short cycle life and the low initial Coulombic efficiency (ICE). In order to address these issues, many strategies have been developed from different aspects, such as structure engineering[10-14], heteroatom doping[15-17], and so on. Among them, the exploration of electrolytes has aroused great interest, because electrolytes directly dictate the interface reactions on electrode materials and then the reversibility of electrochemical reactions. For ester-based electrolytes, the reducing products of ester molecules always lead to a thick but

stable solid-electrolyte-interphase (SEI) film[18-22], thereby offering a reliable protection to hard carbon in NIBs. However, the thick and organic-rich SEI film also lowers the ICEs and rate capability. Different from the case of ester-based electrolytes, ether-based ones form a thin and inorganic-rich SEI film, thus resulting in the improved ICEs and rate capability[23-29]. Using $NaCF_3SO_3$ in diglyme as an electrolyte, reduced graphene oxide (rGO) exhibited a high ICE of 74.5%, an impressive rate capability (~196 mAh g^{-1} at 5 A g^{-1}), and an excellent cycling stability (75.2% after 1000 cycles at 1 A g^{-1})[23]. The ICE could be promoted up to 91.2% by flexible hard carbon papers as a self-supporting anode[24], but the rate capability was slightly reduced to ~170 mAh g^{-1} at 2 A g^{-1}. Xu et. al. tried different methods to realize the merits of ester- and ether- based electrolytes simultaneously for hard carbons, such as a pre-forming SEI film from ester-based electrolytes cycled in ether[25], and the addition of a trace of ester into ether-based electrolytes[26].

Although using ether-based electrolytes to improve the electrochemical performances of HC has been demonstrated, there are still many doubts about the underlying mechanism. The first one is if there is a SEI film on the surface of HC upon cycling. So far, the related discussions about the SEI film are based on X-ray photoelectron spectra (XPS) spectra of cycled electrodes, in which the signals from organic species, -C-O-C-, -(C=O)-, -(C=O)-O-, etc., could be easily visualized[23-26]. Thus, the formation of a SEI film via electrolyte decomposition is concluded. However, the electrode surface, especially those after cycles, is easily contaminated by adsorbed solvents and highly active air/moisture during the cleaning, storage and transfer process of the electrodes. Moreover, the XPS signals from organic binders and conductive carbon can not be effectively excluded. Therefore, this conclusion still needs more evidences from other techniques. Moreover, some works on Na-storage properties of graphite suggest that the reduced products were soluble in the case of ether-based electrolytes[30-32], thus no SEI film was detected. Although HC and graphite have some differences in structures, they still share the similar element, unique graphene layers, and so on. Thus, it is also possible for HC to exhibit a similar electrochemical feature. The second debate is if there is a co-intercalation chemistry in ether-based electrolytes for HC. Although SEI film definitely suppresses the co-intercalation reactions, these reactions still possibly occur[33], because a thin SEI film can be broken at some sites due to the large volume expansion.

In this work, the intercalation chemistry on HC in NIBs is carefully investigated for Na storage. First of all, it is demonstrated that hard carbon exhibits the better electrochemical performances in diglyme (DGM) than that in ethylene carbonate /diethyl carbonate (EC/DEC), in all the important terms, *i.e.* Coulombic efficiency, reversible capacity, cycling stability and rate capability. It can sustain a capacity of 224.4 mAh g^{-1} after 3500 cycles at 1 A g^{-1}. Then, *ex-situ* nuclear magnetic resonance (NMR), gas chromatography-mass spectrometry (GC-MS) and high-resolution transmission electron microscope (HRTEM) were used to clarify the existence of a SEI film on HC or not. These results indicate that there are the marked electrolyte decomposition and the formation of a SEI film in EC/DEC, in line with the previous works. However, what's surprising is no formation of a SEI film in the case of diglyme, which well explains the improved ICE and rate capability. *In-situ* electrochemical quartz crystal microbalance (EQCM) confirms that ether molecules

have been co-intercalated into HC likely in terms of $[Na(DGM)]^+$. To our knowledge, these results are reported for the first time on HC. It might be very useful for us to rational design advanced electrode materials based HC in future.

Results

Electrochemical performances of HC in different electrolytes. DGM is selected as a model to illustrate the unique feature of Na insertion/extraction in HC. Meanwhile, the conventional solvent, EC/DEC, is also tested under the same conditions as the benchmark. Commercial hard carbon is directly used without further treatment. Scanning electron microscopy (SEM) and transmission electron microscope (TEM) images show that they are irregular microparticles with randomly-oriented and intermittent lattice fringes (Supplementary Fig. S1)[34,35]. A variety of structure defects in the particle offer numerous active sites for Na storage. Figure 1 presents the electrochemical performances of HC in DGM and in EC/DEC at 0.1 A g^{-1}. The differences between them are very obvious, particularly in terms of Coulombic efficiency and rate performances. As shown in Figs. 1a and 1b, hard carbon in DGM exhibits a higher ICE (~80.0%) than that in EC/DEC (~68.2%), indicating the reduced side reactions. To gain more information about these side reactions, dQ/dV is plotted against the cell voltage for two cases. HC in EC/DEC gives three cathodic peaks at 0.9 V, 0.5 V and 0.1 V in the first cycle (Fig. 1c), which could be assigned to the adsorption of Na^+ ions on the edge and/or defects of carbon layers, the electrolyte decomposition and the reduction of Na^+ ions within micro-voids[36-38]. In the following cycles, the two cathodic peaks at 0.9 V and 0.5 V almost disappear, but that at 0.1 V only slightly decreases. This result indicates that the two reactions happened at high voltages are the essential origin for low ICE. Different from the case of EC/DEC, HC in DGM only has two cathodic peaks at 1.0 V and 0.1 V in the first cycle (Fig. 1d). The cathodic peak at 0.5 V is invisible in the profile even in the first cycle, suggesting the absence of electrolyte decomposition. This result is quite interesting and not reported before to the best of our knowledge. More important, the coulombic efficiency of HC in DGM is more stable in the subsequent cycles (Fig. 1e), suggesting the high reaction reversibility. On the other hand, HC in DGM also shows the smaller electrode overpotential (~0.08 V) than that in EC/DEC (~0.15 V) for the redox reaction at 0.1 V. It indicates the fast electrochemical reaction kinetics. This conclusion is also supported by rate performances (Fig. 1f). The capacity difference between DGM and EC/DEC increases as the current density arises. At 2 A g^{-1}, the specific capacity of HC remains ~266 mAh g^{-1} in DGM, but only ~15 mAh g^{-1} in EC/ DEC. Even in terms of capacity retention, it still comes to the same conclusion, 78% in DGM vs. 5.9% in EC/DEC. The improvements in reaction kinetics and reaction reversibility do not come at the expense of cycling stability. HC displays a good cycling stability and a large specific capacity in DGM (Fig. 1g). It delivers a capacity of 230 mAh g^{-1} after 1500 cycles at 1 A g^{-1}, much higher than ~40 mAh g^{-1} in EC/DEC. Even after 3500 cycles, the capacity is still 224.4 mAh g^{-1}, corresponding to a capacity retention of 88% (Fig. 1h and Supplementary Fig. S2). It is almost the best performance for hard carbon (Tab. S1).

***Ex-situ* HRTEM images characterization of SEI films.** All these data confirm that the electrochemical performances of HC are remarkably improved in DGM, as compared to the case in EC/DEC. Usually, these

improvements are attributed to the SEI film in different electrolytes[39]. However, the cathodic peak related to the electrolyte decomposition is absent in DGM, even in the first cycle (Fig. 1c). Therefore, it is likely without a SEI film on HC in DGM. Then, the previous explanation based on the SEI film does not work for HC. So, it is important to clarify if there is a SEI film on HC cycled in DGM. HRTEM is an intuitive tool to visualize the SEI film. As shown in Fig. 2a, the surface of hard carbon discharged to 0.01 V is clear without an amorphous layer, thus excluding the formation of a SEI film. The result is in good agreement with that observed in dQ/dV. The intermittent lattice near the surface is a characteristic of HC (Fig. 2b). The fringe spacing about 3.94 Å is larger than that before discharge (~3.6 Å, Supplementary Fig. S1), probably caused by the intercalation of Na ions. As hard carbon is charged to 1.5 V, the similar surface is also observed (Fig. 2c), confirming the non-SEI film again. Meanwhile, the fringe spacing is reduced to ~3.74 Å (Fig. 2c), likely due to Na extraction. The similar surface without a SEI film is also identified after 5 cycles in DGM (Supplementary Figs. S3a and S4a), suggesting the good surface stability. In contrast, the surface of HC cycled in EC/DEC is coated by a thin SEI film, as highlighted in Figs. 2d-2f. The lattice fringes of HC do not show up any more. The contrast differences indicate that the spherical inorganics are randomly dispersed in organic species, resulting in this unique composite. This result is well consistent with the well-accepted Mosaic model about SEI film[40,41]. Unfortunately, the structure information of spherical inorganics is missed, due to the high-energy electron irradiation. In addition, the surface film is not uniform, which affects the local Na-ion flux, increases the stress accumulation and degrades the electrochemical performances. Therefore, after 5 cycles, the surface film on hard carbon becomes much thicker (Supplementary Figs. S3b and S4a), but the internal structure remains as the same.

***Ex-situ* ^{1}H NMR and GC-MS studies on HC.** Although HRTEM gives strong evidences to support the absence of a SEI film on hard carbon in DGM, the detection area by HRTEM is always limited. Moreover, the sample preparation for TEM images may interfere with the identification of the SEI film. So, to avoid the possible misleading by the limitation of TEM, using other techniques to characterize the electrode surface is very necessary. In this context, NMR and GC-MS, which are very good at the detection and characterization of organics, are used[42]. Once there is electrolyte decomposition, the formation of organics is inevitable in the SEI film. The electrodes discharged to different voltages were soaked in deuterated dimethyl sulfoxide (DMSO-d_6) overnight. Due to the strong polarity of DMSO, organics were easily dissolved and the solution was subject to NMR. As illustrated in Fig. 3a, the ^{1}H NMR spectra are kept exactly the same as the standard spectrum of DGM (Supplementary Fig. S5a) throughout the whole discharge process. This result indicates DGM just adsorbs on the surface of hard carbon. This same result is also obtained in ^{13}C NMR, where both the chemical shift and the relative ratio of the signals remain as the same at different voltages (Supplementary Fig. S6). This result excludes the polymerization reaction potentially happened to DGM. In contrast, the ^{1}H spectra of hard carbon

in EC/DEC become totally different (Fig. 3b). The ^{1}H NMR spectrum at OCV is similar to the standard spectrum of EC/DEC (Supplementary Fig. S5b). As the voltage decreases to 0.75 V, the weak chemical shift of sodium ethylene dicarbonate (SEDC) at 3.40 ppm appears in the spectrum[43]. The signal intensity

greatly increases within 0.1-0.01 V, implying the formation of a large amount of SEDC in this voltage range. Beside SEDC, the chemical shift from CH_2 of ethylene also shows up at 0.1 V and intensifies at 0.01 V. The formation of SEDC and ethylene can be attributed to two-molecule polymerization of ethylene carbonate (Supplementary Fig. S7, *Equ.* 1), as supported by their close signal areas. It is noted that the electrolysis products of diethyl carbonate (DEC), *i.e.* sodium methyl carbonate (SMC) and butane (Supplementary Fig. S7, *Equ.* 2), also appear at 0.01 V, despite of the low contents. The appearance of these organic species confirms severe electrolyte decomposition in EC/DEC. The similar changes are also identified in the ^{13}C spectra of hard carbon in EC/DEC (Supplementary Fig. S8).

The conclusion on the basis of GC-MS is similar to that from NMR. Different from the electrode processing for NMR, the electrode for GC-MS was treated by $CDCl_3$, instead of DMSO. The difference of $CHCl_3$ and DMSO in polarity allows them to dissolve different organics, thereby providing another perspective to validate the conclusion. The electrode cycled in DGM exhibits the same fragmentation pattern as that of DGM (Supplementary Fig. S9), where the ions at m/z 29,45,59 and 89 can be assigned to the fragments of DGM caused by electron ionization (EI) (Fig. 3c), *i.e.* $[CH_3CH_2]^+$, $[HOCH_2CH_2]^+$, $[CH_3OCH_2CH_2]^+$, and $[HOCH_2CH_2OCH_2CH_2]^+$. This result indicates that there are some DGM molecules adsorbed on the electrode surface, which cannot be removed by simple washing. As expected, the fragment pattern remains almost identical at the different voltages, indicating the good stability of the electrolytes and the absence of SEI film on the surface. The same result is even observed in the electrode discharged to 0.01 V after three cycles (Supplementary Fig. S10). On the contrary, the electrode cycled in EC/DEC exhibit the different fragmentation patterns, as the discharging undergoes. A batch of new fragment ions at m/z > 90 appears in the fully-discharged electrode (Fig. 3d), indicating the formation of new organics (e. g. SEDC at m/z 148) in the electrode. This result can be attributed to the electrolyte decomposition at a low voltage, which is also in good agreement with what observed in NMR.

***In situ* EQCM of HC in DGM.** *In-situ* EQCM allows us to accurately monitor the tiny weight change of the electrodes as a function of the applied voltages. Therefore, it can provide useful information about the formation of the SEI film and the intercalation of Na^+ into the electrodes, because both of them involve the mass gain or loss in the electrodes[44]. In a typical experiment, the electrodes are discharged either in DGM or in EC/DEC at a constant current density in a specially designed cell, using Na as the reference electrode. As shown in Fig. 4a, the voltage quickly falls to -2.65 V (vs. Ag^+/Ag) and then gradually approaches -2.8 V (vs. Ag^+/Ag) during discharging, which indicates the adsorption and insertion of Na^+ into hard carbon. Fig. 4b shows the plot of mass vs. charge, where two stages can be clearly seen. During the first stage, the mass change per electron, $\Delta m/dq$, is 24.6 g mol^{-1}, which is close to the ionic mass of Na^+ (23 g mol^{-1}) indicating that the adsorption of Na^+ ions on hard carbon, probably at the edges or structure defects of carbon layers. During the second stage, $\Delta m/dq$ increases to 160.3 g mol^{-1} until the end of the discharging. This result is consistent with the mass/charge ratio of $[Na(DGM)]^+$ (157 g mol^{-1}), implying that the solvent molecules are intercalated into hard carbon together with Na^+ ions. Interestingly, the carbon layers are not exfoliated upon the intercalation of the organic molecules, because the

graphene domains in hard carbon are randomly-oriented and intermittent. Thus, the graphene layer won't be easily peeled off and detached from the others. As a result, hard carbon exhibits a stable cycling over 3500 cycles, as demonstrated in Fig. 1h. Moreover, the mass/charge ratios related to the SEI components, such as polyDGMs, sodium alkyl alcohol (RCONa), etc. are not observed. It excludes the formation of a SEI film on hard carbon again, consistent with the results from NMR, MS and HRTEM. To our knowledge, these results, especially the identification of solvent molecules in hard carbon, are reported for the first time. The height change with charge as shown in Fig. 4c is consistent with the weight change in Fig. 4b, indicating that the adsorption and the intercalation of Na-related species make the electrode expanded accordingly.

Molecular dynamics simulations. To further understand the co-intercalation of DGM with Na^+ into hard carbons, the solvated structures of $NaPF_6$ in DGM are simulated by molecular dynamics (MD) based on first-principle theory[45-47]. As illustrated in Fig. 4d, a supercell contains 16 DGM molecules, one Na^+ ion and one PF_6^- ion, keeping in line with a low concentration of $NaPF_6$ in DGM. The cell was then heated to 1000 K and 2000 K in turn. At each temperature, MD simulations were conducted for 1 ps with a time step of 0.25 fs to identify the thermodynamically stable configuration. Then, the cell was cooled to room temperature by velocity scaling. After that, the cell was treated by NVT simulation at 300 K for 10 ps. (full name of NVT) Then, it is noted that each Na ions are surrounded by six O atoms. Three of them come from the same DGM molecule, while the other three originate from three different DGM molecules. In this context, the three molecules are easy to dissociate from Na ions, because they are only a monodentate ligand. The DGM molecule binding to Na ions with three O atoms is co-intercalated together in to hard carbon. This configuration is quite stable in DGM, as supported by the trajectories of all O atoms in the cells (Fig. 4f). This result provides the solid basis for the co-intercalation of DGM with Na ions into hard carbon. The same conclusion could be also obtained in the cases of graphite and soft carbon. As shown in HRTEM images (Supplementary Fig. S11), all the particle surfaces after 5 cycles exhibit clear lattice fringes without a sign of a SEI film. These results strongly confirm the absence of a SEI film.

Discussion

In conclusion, intercalation chemistry of hard carbon in ether-based electrolytes is carefully investigated for Na storage using ester-based electrolytes as the benchmark. It is noted that hard carbon exhibits the better electrochemical performances in ether than that in ester, in all the important terms, *i.e.* coulombic efficiency, reversible capacity, cycling stability and rate capability. It can sustain a capacity of 224.4 mAh g^{-1} after 3500 cycles at 1 A g^{-1}. More exciting, ex-situ NMR, MS and HRTEM support the absence of a SEI film on the surface of hard carbon. In contrast, there is the severe decomposition of electrolyte and the formation of a SEI film in ester. ECQM reveals that the intercalation of Na^+ into hard carbon is accompanied by one molecule of ether, $[Na(DGM)]^+$. The incomplete dissociation of ether from solvated Na^+ lowers the energy barrier, and facilitate the fast intercalation/deintercalation. The absence of a SEI film increases the coulombic efficiency and rate capability. The absence of a SEI film can be attributed to

the high stability of solvated Na^+ ions, as indicated by DFT calculations. Finally, the similar phenomenon is also observed in graphite and soft carbon.

Methods

Hard carbon was bought from Kuraray Co. Ltd.

Electrochemical measurements. Electrochemical performances of hard carbons as the anode material for NIBs were tested in CR2032-type coin cells. First of all, hard carbons, acetylene black (AB) and sodium alginate (SA) were mixed in a weight ratio of 7:2:1. Then, several drops of distilled water were added into the mixture. After ground for 30 min by hands, the resultant slurry was spread on a copper foil by a doctor blade, followed by drying in vacuum at 60 ^oC for 12 h. Then, the foil was punched into the discs with a diameter of ~12 mm. In this case, the mass loading of the active materials on the discs was about 1.5-2.5 mg cm^{-2}. The disc was used as the working electrode and assembled with Na metal as the counter electrode, and glass fiber (Celgard 2325) as the separator in an Ar-filled grove box (Mikrouna, Super 1220/750/900, H_2O<1ppm; O_2<1ppm). Two different electrolytes, 1.0 M $NaPF_6$ in diglyme or in EC/DEC, were examined to illustrate their differences. Galvanostatic discharge/charge profiles were performed on a battery cycler (LAND CT-2001A, China) at room temperature. Cyclic voltammetry (CV) were conducted on an electrochemical workstation (Chenghua CHI 760E, China) at room temperature. Electrochemical impedance spectra (EIS) were obtained from an electrochemical workstation (Autolab PGSTAT 302N, Switzerland) in a frequency range of 100 KHz to 0.01Hz.

Characterization of SEI film. *Ex-situ* NMR and GC-MS. The electrodes tested for NMR and MS were discharged/charged for five cycles at 0.05 A g^{-1}. Then, the cells stabilized at different voltages. After that, the electrodes were taken out from coin cells, placed in centrifuge tubes and soaked either in DMSO-d_6 for $^1H/^{13}C$ NMR or in D_2O for ^{23}Na NMR. The centrifuge tubes were sealed and sonicated about 30 min to ensure the organics in the SEI film to dissolve as much as possible. Finally, the supernatant was transferred into NMR tubes, and sealed air-tightly for NMR. NMR spectra were achieved with an advanced spectrometer (Bruker AVANCE III 500, Germany), using DMSO-d_6 at 2.500 ppm for $^1H/^{13}C$ NMR, or NaCl in D_2O at 0 ppm for ^{23}Na NMR. For MS, DMSO-d_6 was replaced by $CDCl_3$ and the other was kept as the same. MS was conducted on a gas chromatography- mass spectrometer (GC MS-TQ8040 NX, Shimadzu, Japan).

***Ex-situ* TEM and SEM images.** First, the electrodes were discharged/charged for five cycles at 0.05 A g^{-1}. Then, the electrode was discharged to 0.01 V or charged to 1.5 V to identify the surface of HC. The working electrode was taken out from coin cells and washed several times with absolute ethanol. Electrode materials was scraped from the current collector, dispersed in absolute ethanol and sonicated for tens of minutes. Finally, a small droplet of the suspension was dropped on a porous carbon-coated copper grid for TEM images. TEM images, HRTEM images, high-angle annular dark-field scanning TEM (HAADF-STEM) images, X-ray energy-dispersive spectrum (EDS) and element maps were recorded with an

aberration-corrected TEM microscope (FEI Tecnai F20, USA). SEM images were acquired from a field-emission scanning electron microscope (Zeiss Gemini 300, Germany).

***In-situ* EQCM.** EQCM measurements were performed using an electrochemical work station (Chenghua CHI 760E, China) coupled with a Q-Sense instrument (Baolin Scientific, Sweden). A AT-cut quartz crystal coated by gold (Q-Sense Sensor QSX 338 Gold), a Pt filament and an aqueous solution of $Ag/AgNO_3$ were used as the working electrode, the counter electrode and the reference electrode. The measurement was carried out at a current density of 50 uA in the range of (-1.423/-2.923 V vs. $Ag/AgNO_3$), using a standard three-electrode configuration. Hard carbon was deposited on the working electrode by a spin coater. The mass change (Δm) of the working electrode followed the Sauerbrey equation.

Computational Method. Molecular dynamics simulations based on density functional theory were carried out with the Perdew-Burke-Ernzerhof (PBE) exchange-correlation functional[48] as implemented in the Vienna Ab initio Simulation Package (VASP)[49]. The projector augmented wave potentials[50] were used with plane-wave basis set. The plane-wave cutoff energy was set to be 340 eV. For setting up the supercell, the experimental density of 0.944 g/cm^3 was used. The Γ-point was used to represent the Brillouin zone. The Nosé thermostat[51] was used to regulate the temperature in NVT simulation.

Declarations

Data availability. The authors declare that the data supporting the findings of this study are available within the article and its Supplementary Information files.

ACKNOWLEDGEMENT

We thank the financial support from National Nature Science Foundation of China (21971146, 21871008), Taishan Scholarship in Shandong Provinces (ts201511 004), Science, Technology and Innovation Commission of Shenzhen Municipality (JCYJ20180305 164424922), Fundamental Research Funds of Shandong University (2018JC023), The Key Research Program of Frontier Sciences, Chinese Academy of Sciences (QYZDJ-SSW-JSC013) and Super Post Doctoral Fellow Program of Shanghai (E01SCB17). We also acknowledge the assistance of Shandong University Structural Constituent and Physical Property Research Facilities. We thank Dr. Jiong Jia for his support with nuclear magnetic resonance (500 M) and thank Dr. Heliang Yao is helpful for the transmission electron microscope observations.

Author contributions

J.P. conceived the experiment. J.P. and Y.H.Y. conducted the material synthesis, characterization and electrochemical measurement. L.F. carried out the *ex-situ* GC-MS experiments. Y.F.Z. performed the *in-situ* EQCM test. A.M.L. conducted the theoretical calculation and analyzed the related data with the guidance of Y.Y.S. J.Y., F.Q.H. wrote the manuscript with further inputs from other authors.

Competing financial interests: The authors declare no competing financial interests.

References

1. Matthew, L., Jun, L., Chen, Z. W. & Amine, K. 30 years of lithium-ion batteries. *Adv. Mater.* **30,** 1800561 (2018).
2. Assat, G. & Tarascon, J. M. Fundamental understanding and practical challenges of anionic redox activity in Li-ion batteries. *Nature Energy* **3,** 373-386 (2018).
3. Lin, L. D., Xu, X. N., Chu, C. X., Majeed, M. K. & Yang, J. Mesoporous amorphous Si: a simple synthesis to high-rate and long-life anode material for lithium ion batteries. *Angew. Chem. Int. Ed.* ***55,*** 14063-14066 (2016).
4. Li, L., Zheng, Y., Zhang, S. L., Yang, J. P., Shao, Z. P. & Guo, Z. P. Recent progress on sodium ion batteries: potential high-performance anodes. *Energy Environ. Sci.* **11,** 2310-2340 (2018).
5. C. Delmas, Sodium and sodium-ion batteries: 50 years of research. *Adv. Energy Mater.* **8,** 1703137 (2018).
6. Hwang, J. Y., Myung, S. T. & Sun, Y. K. Sodium-ion batteries: present and future. *Chem. Soc. Rev.* **46,** 3529-3614 (2017).
7. Hou, H. S., Qiu, X. Q., Wei, W. F., Zhang, Y. & Ji, X. B. Carbon anode materials for advanced sodium-ion batteries. *Adv. Energy Mater.* **7,** 1602898 (2017).
8. Jache, B. & P. Adelhelm, Use of graphite as a highly reversible electrode with superior cycle life for sodium-ion batteries by making use of co-intercalation phenomena. *Angew. Chem. Int. Ed.* **53,** 10169-10173 (2014).
9. Kim, H. et al. Sodium intercalation chemistry in graphite. *Energy Environ. Sci.* **8,** 2963-2969 (2015).
10. Dou, X. W. et al. Impact of the acid treatment on lignocellulosic biomass hard carbon for sodium-ion battery anodes. *ChemSusChem* **11,** 3276-3285 (2018).
11. Xiang, J. Y., Lv, W. M., Mu, C. P., Zhao, J. & Wang, B. C. Activated hard carbon from orange peel for lithium/sodium ion battery anode with long cycle life. *J. Alloys Compd.* **701,** 870-874 (2017).
12. Xiao, L.F. et al. Hard carbon nanoparticles as high-capacity, high-stability anodic materials for Na-ion batteries. *Nano Energy* **19,** 279-288 (2016)
13. Zhang, N. et al. High capacity hard carbon derived from lotus stem as anode for sodium ion Batteries, *J. Power Sources* **378,** 331-337 (2018).
14. Zhang, Y. J. et al. Honeycomb-like hard carbon derived from pine pollen as high-performance anode material for sodium-ion batteries. *ACS Appl. Mater. Interfaces* **10,** 42796-42803 (2018).
15. Li, Z. F. et al. Defective hard carbon anode for Na-ion batteries. *Chem. Mater.* **30,** 4536-4542 (2018).
16. Wu, F. et al. Expanding interlayer spacing of hard carbon by natural K^+ doping to boost Na-ion storage. *ACS Appl. Mater. Interfaces* **10,** 27030-27038 (2018).

17. Li, Y. et al. Insights into the Na^+ storage mechanism of phosphorus-functionalized hard carbon as ultrahigh capacity anodes. *Adv. Energy Mater.* **8,** 1702781 (2018)
18. Soto, F. A. et al. Tuning the solid electrolyte interphase for selective Li- and Na-ion storage in hard carbon. *Adv. Mater.* **29,** 1606860 (2017).
19. Patra, J. et al. Moderately concentrated electrolyte improves solid-electrolyte interphase and sodium storage performance of hard carbon. *Energy Storage Mater.* **16,** 146-154 (2019)
20. Kim, D. H., Kang, B. S. & Lee, H. C. Comparative study of fluoroethylene carbonate and succinic anhydride as electrolyte additive for hard carbon anodes of Na-ion batteries. *J. Power Sources* **423,** 137-143 (2019)
21. Liu, X. W. et al. High capacity and cycle-stable hard carbon anode for nonflammable sodium-ion batteries. *ACS Appl. Mater. Interfaces* **10,** 38141-38150 (2018).
22. Komaba, S. et al. Electrochemical Na insertion and solid electrolyte interphase for hard-carbon electrodes and application to Na-ion batteries. *Adv. Funct. Mater.* **21,** 3859-3867 (2011).
23. Zhang, J. et al. Achieving superb sodium storage performance on carbon anodes through an ether-derived solid electrolyte interphase. *Energy Environ. Sci.* **10,** 370-376 (2017).
24. Hou, B. H. et al. Self-supporting, flexible, additive-free, and scalable hard carbon paper self-interwoven by 1D microbelts: superb room/low-temperature sodium storage and working mechanism. *Adv. Mater.* **31,** 1903125 (2019).
25. Bai, P. X. et al. Long cycle life and high rate sodium-ion chemistry for hard carbon anodes. *Energy Storage Mater.* **13,** 274-282 (2018).
26. Bai, P. X. et al. Solid electrolyte interphase manipulation towards highly stable hard carbon anodes for sodium ion batteries. *Energy Storage Mater.* **25,** 324-333 (2020).
27. Zhu, Y. E. et al. Boosting the rate capability of hard carbon with an ether-based electrolyte for sodium ion batteries. *J. Mater. Chem. A* **5,** 9528-9532 (2017).
28. Xiao, W. et al. Utilizing the full capacity of carbon black as anode for Na-ion batteries via solvent co-intercalation. *Nano Res.* **10,** 4378-4387 (2017).
29. Zhou, Y. F. et al. Real-time mass spectrometric characterization of the solid-electrolyte interphase of a lithium-ion battery. *Nat. Nanotech.* **15,** 224-230 (2020).
30. Jache, B., Binder, J. O., Abe, T. & Adelhelm, P. A comparative study on the impact of different glymes and their derivatives as electrolyte solvents for graphite co-intercalation electrodes in lithium-ion and sodium-ion batteries. *Phys. Chem. Chem. Phys.* **18,** 14299-14316 (2016).
31. Goktas, M. et al. Graphite as cointercalation electrode for sodium-ion batteries: electrode dynamics and the missing solid electrolyte interphase (SEI). *Adv. Energy Mater.* **8,** 1702724 (2018).
32. Kim, Y. et al. Revisiting solid electrolyte interphase on the carbonaceous electrodes using soft X-ray absorption spectroscopy. *ACS Appl. Mater. Interfaces* **10,** 29992-29999 (2018).
33. Maibach, J., Jeschull, F., Brandell, D., Edstrom, K. & Valvo, M. Surface layer evolution on graphite during electrochemical sodium-tetraglyme co-intercalation. *ACS Appl. Mater. Interfaces* **9,**

12373–12381 (2017).

34. Wang, Q. Q. et al. Rice husk-derived hard carbons as high-performance anode materials for sodium-ion batteries. *Carbon* **127,** 658-666 (2018).
35. Zheng, Y. H., Wang, Y. S., Lu, Y. X., Hu, Y. S. & Lu, J. A high-performance sodium-ion battery enhanced by macadamia shell derived hard carbon anode. *Nano Energy* **39,** 489-498 (2017).
36. Ghimbu, C. M. et al. Insights on the Na^+ ion storage mechanism in hard carbon: Discrimination between the porosity, surface functional groups and defects. *Nano Energy* 44, 327-335 (2018).
37. Reddy, M. A., Helen, M., Groß, A., Fichtner, M. & Euchner, H. Insight into Sodium Insertion and the Storage Mechanism in Hard Carbon. *ACS Energy Lett.* **3,** 2851-2857 (2018).
38. Sun, N. et al. Extended adsorption-insertion" model: a new insight into the sodium storage mechanism of hard carbons. *Adv. Energy Mater.* **9,** 1901351. (2019).
39. He, Y. W., Bai, P. X., Gao, S. Y. & Xu, Y. H. Marriage of an ether-based electrolyte with hard carbon anodes creates superior sodium-ion batteries with high mass loading. A*CS Appl. Mater. Interfaces* **10,** 41380-41388 (2018).
40. Cao, X. et al. Monolithic solid-electrolyte interphases formed in fluorinated orthoformate-based electrolytes minimize Li depletion and pulverization. *Nature Energy* **4,** 796-805 (2019).
41. Li, K. K. et al. Evolution of the electrochemical interface in sodium ion batteries with ether electrolytes. *Nat. Commun*. **10,** 1248 (2019).
42. Hope, M. A. et al. Selective NMR observation of the SEI-metal interface by dynamic nuclear polarization from lithium metal. *Nat. Commun*. **11,** 2224 (2020).
43. Wang, L. N. et al. Identifying the components of the solid-electrolyte interphase in Li-ion batteries. *Nat. Chem.* **11,** 789-796 (2019).
44. Liu, T. C. et al. In situ quantification of interphasial chemistry in Li-ion battery. *Nat. Nanotech.* **14,** 50-56 (2019).
45. Liu, M. Z. et al. Deciphering the paradox between the co-intercalation of sodium-solvent into graphite and its irreversible capacity. *Energy Storage Materials* **26,** 32-39 (2020).
46. Zhou, L. et al. Electrolyte engineering enables high stability and capacity alloying anodes for sodium and potassium ion batteries. *ACS Energy Lett.* **5,** 766-776 (2020).
47. Wang, C. et al. Overlooked electrolyte destabilization by manganese (II) in lithium-ion batteries. *Nat. Commun*. **10,** 3423 (2019).
48. Perdew, J. P., Burke, K. & Ernzerhof, M. Generalized gradient approximation made simple. *Phys. Rev. Lett.* **77,** 3865-3868 (1996).
49. Kresse, G. & Furthmuller, J. Efficiency of ab-initio total energy calculations for metals and semiconductors using a plane-wave basis set. *Comput. Mater. Sci.* **6,** 15-50 (1996).
50. Kresse, G. & Joubert, D. From ultrasoft pseudopotentials to the projector augmented-wave method. *Phys. Rev. B* **59,** 1758-1775 (1999).

51. Nosé, S. A unified formulation of the constant temperature molecular dynamics methods. *J. Chem. Phys.* **81,** 511-519 (1984).

Figures

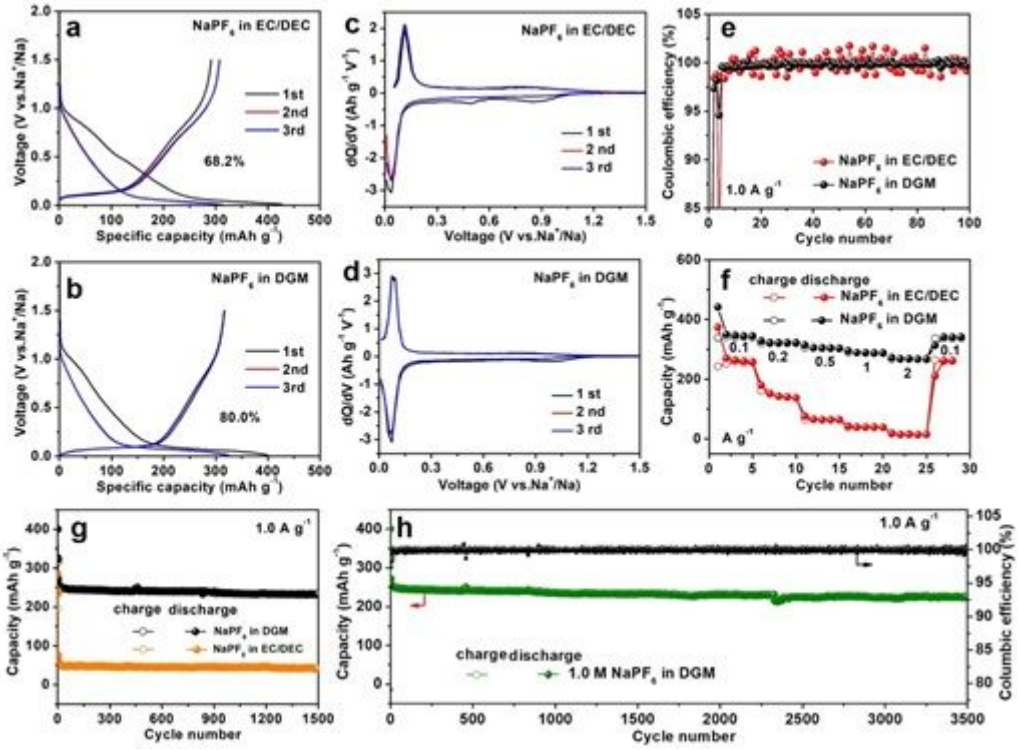

Figure 1

Electrochemical performances of hard carbon in different electrolytes. Galvanostatic discharge/charge curves in EC/DEC (a) and in DGM (b); dQ/dV plots in EC/DEC (c) and in DGM (d); Coulombic efficiency (e), rate performances (f) and cycling performances (g) in EC/DEC and in DGM; Long-cycling performance of hard carbon in DGM (h).

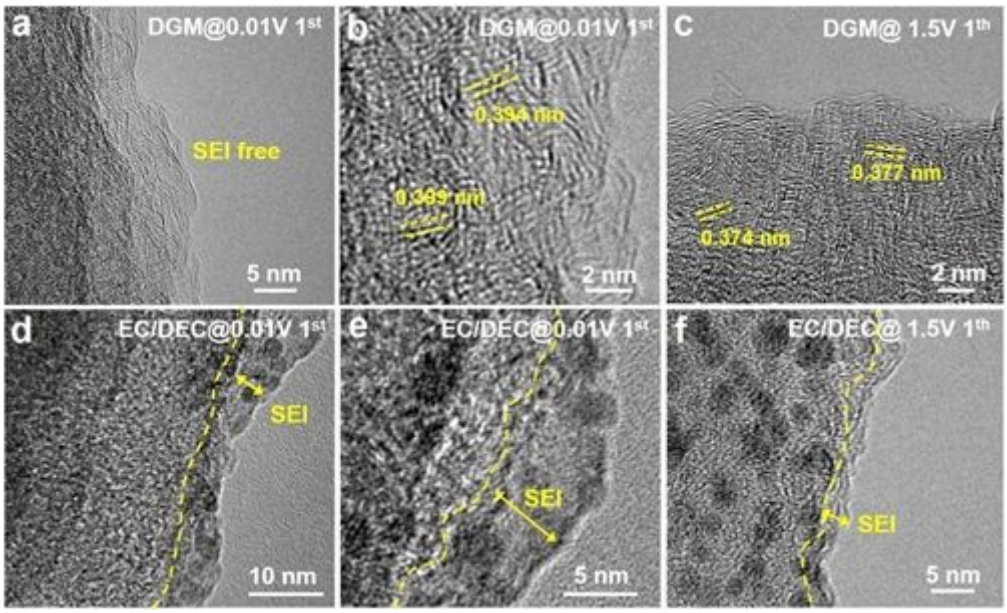

Figure 2

Ex-situ HRTEM images characterization. HRTEM images of HC cycled in DGM (a-c) or in EC/DEC (d-f) during the first cycle. (a, b, d, e) 0.01 V; (c, f) 1.5 V.

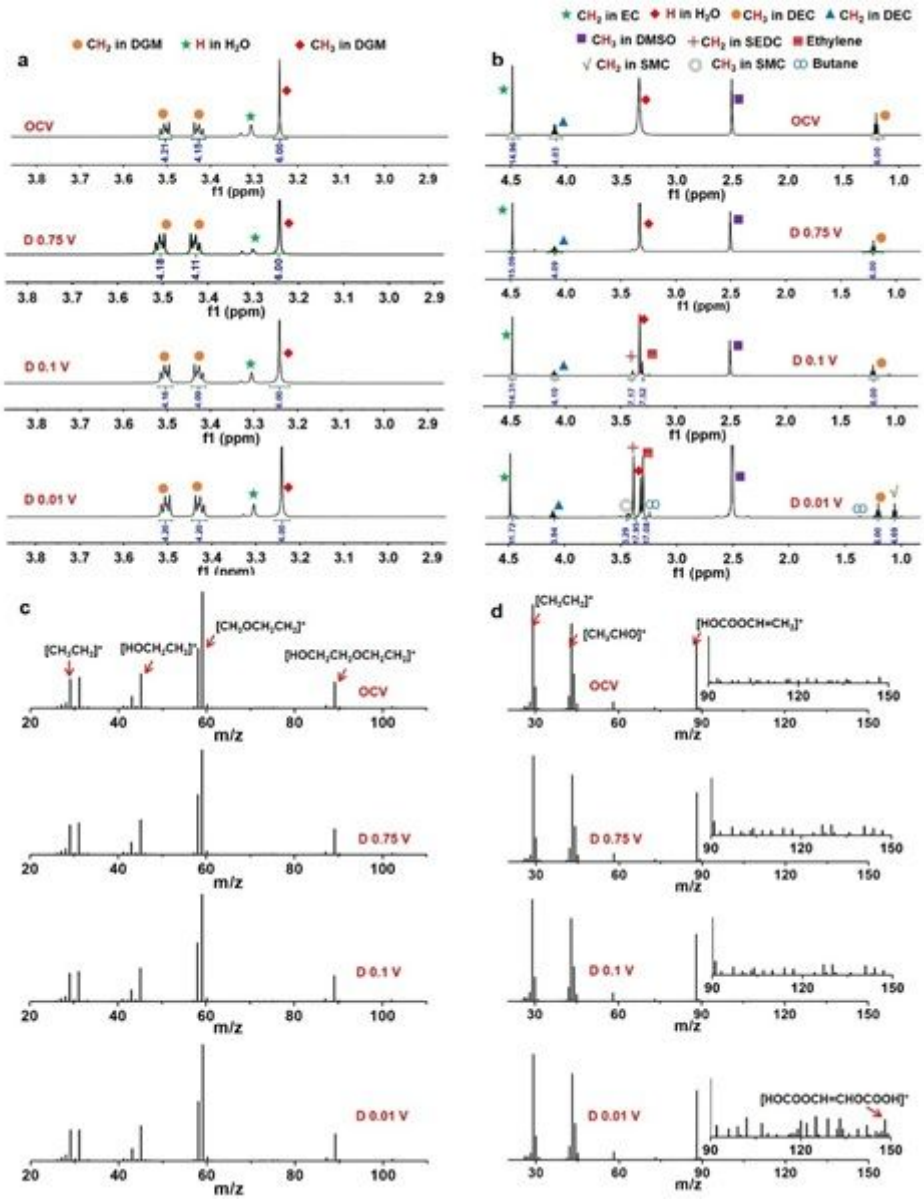

Figure 3

Ex-situ 1H NMR and GC-MS studies on hard carbon. In DGM (a, c) and EC/DEC (b, d) at different discharge voltages.

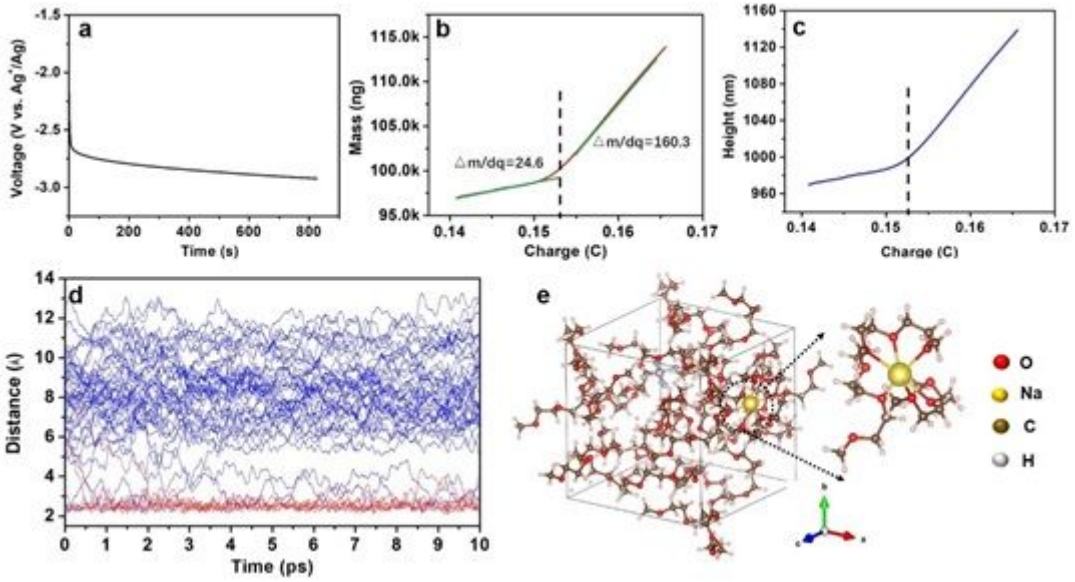

Figure 4

In situ quantitative characterization of live formation and chemistry of hard carbon in DGM. (a) Discharge curves. (b, c) Matched mass and height change during the discharge process. (d) The distance between each O atom and Na ion during the 40,000-step molecular dynamics simulation. (e) The interaction between DGM solvent and Na+ ions.

Supplementary Files

This is a list of supplementary files associated with this preprint. Click to download.

- SI.docx
- GraphicalAbstract.pdf